Langmuir Article

pubs.acs.org/Langmuir

Dye-Sensitized Solar Cells: Driving-Force Effects on Electron Recombination Dynamics with Cobalt-Based Shuttles

Michael J. DeVries, Michael J. Pellin, and Joseph T. Hupp*

Department of Chemistry, Northwestern University, 2145 Sheridan Road, Evanston, Illinois 60208, and Materials Science Division, Argonne National Laboratory, 9700 S. Cass Ave., Argonne, Illinois 60439

Received December 9, 2009. Revised Manuscript Received January 28, 2010

A series of cobalt-containing redox couples, based on $[Co(1,10\text{-phenanthroline})_3](ClO_4)_2$ and its derivatives, were prepared for use as regenerators/shuttles in dye-sensitized solar cells featuring modified TiO_2 photoelectrodes. Surface modification and trap-state passivation of the TiO_2 nanoparticle film electrodes were accomplished via atomic layer deposition of an ultrathin alumina coating. Electron lifetimes were then extracted from open-circuit voltage decay measurements. Cells employing alumina barrier/passivation layers exhibited higher open-circuit voltages as shuttles with more positive redox potentials were used, with the $Co(5\text{-nitro-phen})_3^{3+/2+}$ couple exhibiting the highest V_{oc} (0.844 V). Analysis of the open-circuit voltages and electron lifetimes indicate Marcus normal-region behavior for back electron transfer from the TiO_2 photoanode to these compounds.

Introduction

The archetypal, high-performance dye-sensitized solar cell (DSSC) introduced by O'Regan and Graetzel in 1991 operates via the collection of photons by a visible-region dye adsorbed onto a high surface area photoanode composed of otherwise transparent TiO_2 nanoparticles.[1−5] An electron is quickly injected from the excited state of the dye into the conduction band of the TiO_2. The oxidized dye is regenerated by a redox shuttle in solution, and the loop is closed by the reduction of the shuttle at a platinized cathode. The dye forms a thin layer (monolayer) on the surface of the semiconductor; in early attempts at sensitization with low surface area photoanodes the monolayer dye configuration allowed for only very modest light absorbance and, therefore, miniscule photocurrents.[6] The early success of O'Regan and Gratzel and the comparatively high efficiencies of what are now referred to as "Gratzel cells" are largely attributable to the high-surface-area photoanode used. While this architecture allows for increased dye adsorption and thus higher photocurrents, it also creates a high-area interface with the redox shuttle. Since the dominant recombination pathway in the best dye-sensitized solar cells is the interception of injected electrons by the oxidized form of the redox shuttle, the high interfacial area leads to large dark currents—the consequence of which is a low open-circuit voltage. To minimize such effects, as well as ensure good charge collection, the use of a redox shuttle with slow electron transfer kinetics at the interface, I_3^-/I^-, is usually necessitated.

A recent perspective article suggested that the most promising routes for improving device performance will be to (a) increase current density by employing dyes that absorb over a greater portion of the solar spectrum and (b) increase open-circuit voltge (V_{oc}) by decreasing the overpotential for dye regeneration.[7] The use of high extinction dyes such as conjugated porphyrins[8−12] and other organic dyes[13−15] absorbing further red, in addition to increasing photocurrent density, may allow for the use of photoanode architectures with lower surface area exposed to the redox shuttle, thereby reducing dark current. The most straightforward way to reduce the overpotential for dye regeneration is to find an alternative to the I_3^-/I^- redox shuttle. This shuttle has a potential that is ~550 mV negative of the $dye^{+/0}$ potential in state-of-the-art Gratzel cells. While it is likely that this shuttle will need to be replaced regardless of its efficiency due to the challenges its corrosive nature and volatility put on maintaining the longevity of commercial modules,[16] an alternative that shares its confluence of desirable kinetics and comparable efficiencies has not yet been found. In addition, the I_3^-/I^- couple reacts via mechanisms that remain unclear but involve transfer of multiple electrons;[17] thus, rational optimization of shuttle performance is difficult, and interest in alternatives has increased.

Ideally, alternative redox shuttles should simultaneously display each of several important behaviors or properties, including

*To whom correspondence should be addressed.

(1) O'Regan, B.; Gratzel, M. *Nature* **1991**, *353*, 737–740.
(2) Ardo, S.; Meyer, G. J. *Chem. Soc. Rev.* **2009**, *38*, 115–164.
(3) Gratzel, M.; Durrant, D. R. *Ser. Photoconvers. Sol. Energy* **2008**, *3*, 503–538.
(4) Peter, L. M. *Phys. Chem. Chem. Phys.* **2007**, *9*, 2630–2642.
(5) Martinson, A. B. F.; Hamann, T. W.; Pellin, M. J.; Hupp, J. T. *Chem.—Eur. J.* **2008**, *14*, 4458–4467.
(6) Matsumura, M.; Nomura, Y.; Tsubomura, H. *Bull. Chem. Soc. Jpn.* **1977**, *50*, 2533–2537.
(7) Hamann, T. W.; Jensen, R. A.; Martinson, A. B. F.; Van Ryswyk, H.; Hupp, J. T. *Energy Environ. Sci.* **2008**, *1*, 66–78.
(8) Kay, A.; Gratzel, M. *J. Phys. Chem.* **1993**, *97*, 6272–6277.
(9) Boschloo, G. K.; Goossens, A. *J. Phys. Chem.* **1996**, *100*, 19489–19494.
(10) Campbell, W. M.; Burrell, A. K.; Officer, D. L.; Jolley, K. W. *Coord. Chem. Rev.* **2004**, *248*, 1363–1379.
(11) Planells, M.; Forneli, A.; Martinez-Ferrero, E.; Sanchez-Diaz, A.; Sarmentero, M. A.; Ballester, P.; Palomares, E.; O'Regan, B. C. *Appl. Phys. Lett.* **2008**, *92*, 153506-1–3.
(12) Lee, C.-W.; Lu, H.-P.; Lan, C.-M.; Huang, Y.-L.; Liang, Y.-R.; Yen, W.-N.; Liu, Y.-C.; Lin, Y.-S.; Diau, E. W.-G.; Yeh, C.-Y. *Chem.—Eur. J.* **2009**, *15*, 1403–1412.
(13) Nazeeruddin, M. K.; Humphry-Baker, R.; Gratzel, M.; Murrer, B. A. *Chem. Commun.* **1998**, 719–720.
(14) Kamat, P. V.; Hotchandani, S.; Lind, M.; Thomas, K. G.; Das, S.; George, M. V. *J. Chem. Soc., Faraday Trans.* **1993**, *89*, 2397–2402.
(15) Sayama, K.; Sugino, M.; Sugihara, H.; Abe, Y.; Arakawa, H. *Chem. Lett.* **1998**, 753–754.
(16) Additionally, the I_3^-/I^- couple appears to be poorly suited to DSSCs that feature highly polarizable organic dyes as sensitizers. Complications due to redox quenching, dye/shuttle complex formation, and dark-current catalysis have been reported. See for example: (a) Splan.; et al. *J. Phys. Chem. B* **2004**, *108*, 4111–4115. (b) Reynal.; et al. *J. Am. Chem. Soc.* **2008**, *130*, 13558–13567. (c) Miyashita.; et al. *J. Am. Chem. Soc.* **2008**, *130*, 17874–17881.
(17) Frank, A. J.; Kopidakis, N.; van de Lagemaat, J. *Coord. Chem. Rev.* **2004**, *248*, 1165–1179.

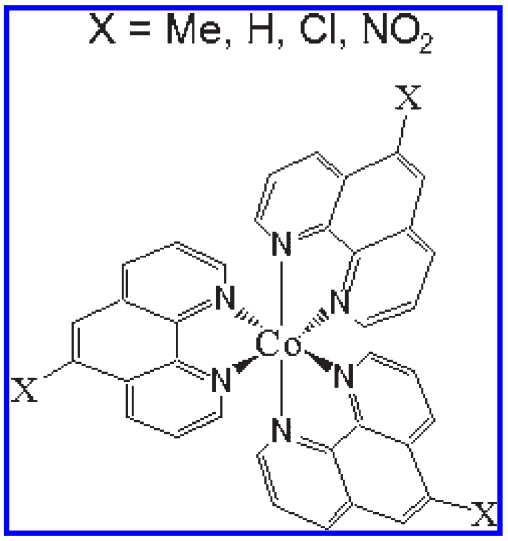

Figure 1. Structure of cobalt complexes (counterions omitted). Substitutions were made in the X position to alter redox potential.

(a) efficient reduction of the dye with minimal overpotential, (b) fast reduction at the cathode, (c) slow interception of electrons contained in the photoanode, (d) nonvolatility, and (e) minimal light absorption. Cobalt polypyridyl couples have attracted attention[18−21] because they seem to have the potential to satisfy all five requirements.[22] In contrast, I_3^-/I^- falls short on requirement (a), while most other shuttles fall short on requirement (c): slow interception of injected electrons. Cobalt(III) complexes are generally anticipated to react slowly with injected electrons on account of a change of spin upon reduction to cobalt(II). The spin change gives rise to large normal-coordinate displacements that are manifest as large vibrational reorganization energies and as large barriers to electron transfer, at least at low and moderate driving forces.

With these observations in mind, we undertook a study of driving-force effects upon the dynamics of the recombination of injected electrons with the cobalt shuttle. To vary the driving force, we introduced electron-withdrawing or -donating groups at the 5-position of 1,10-phenanthroline, thereby altering the Co(III/II) potential (Figure 1). In a previous study,[23] involving ZnO electrodes and $Co(bpy)^{3+/2+}$ (bpy = 2,2′-bipyridine), the driving force was varied by varying the pH of an aqueous solution and thereby shifting the conduction band edge. Additionally, while the present report was in preparation an interesting and closely related paper by Klahr and Hamann appeared.[24] They examined the dynamics of recombination in DSSCs containing various derivatives of $Co(bpy)_3^{3+/2+}$ as shuttles. The motivations for the present study were to gain insight into the fundamentals of the electron interception process and to determine whether the large intrinsic barriers for Co(III/II) electron exchange could be exploited to attain large open-circuit photovoltages with versions of the $Co(phen)_3^{3+/2+}$ couple having far more positive redox potentials. As detailed below, our approach focuses mainly on measurements of current-density/voltage curves and on open-circuit voltage decay (OCVD) assessments of electron survival times.

Experimental Procedure

Electrode Preparation. Photoanodes were prepared on 8 Ω cm^{-2} FTO glass (Hartford Glass). 1.5 × 1.5 cm squares were cut, sonicated in water with detergent for 15 min, and then rinsed with deionized water and ethanol. Electrodes were then heated to 400 °C for 20 min to remove organic residues before depositing a TiO_2 blocking layer with atomic layer deposition. ALD was performed with a Savannah 100 reactor (Cambridge Nanotech, Inc.). TiO_2 blocking layers were deposited over the FTO at 200 °C using titanium isopropoxide (Aldrich) and water as precursors, with a pulse time of 1 s, an exposure time of 1 s, and a nitrogen purge time of 8 s for TIP and a pulse time of 0.1 s, an exposure time of 1 s, and a nitrogen purge time of 15 s for water. 300 cycles were deposited with an approximate growth rate of 0.35 Å/cycle, giving an approximate TiO_2 blocking layer thickness of 10.5 nm.

A transparent TiO_2 nanoparticle layer was made by doctor-blading a TiO_2 nanoparticle paste (DSL 18NR-T, Dyesol) onto the TiO_2-coated FTO glass with a 0.25 cm^2 hole punched into a piece of Scotch tape. Transparent pastes on the electrodes were then dried in an oven at 100 °C for 20 min before doctor-blading a scattering TiO_2 nanoparticle paste (WER4-O, Dyesol) over top of them. The tape was then removed, and the electrodes were annealed in air at 500 °C for 20 min. Immediately following the annealing step, electrodes were coated with 1−5 ALD cycles of alumina at 200 °C using trimethylaluminum and water as precursors, with pulse times of 0.05 and 0.1 s, respectively, exposure times of 15 s, and nitrogen purge times of 30 s. Following ALD, electrodes were cooled to 80 °C and immersed in a 0.5 mM solution of [Ru(4,4′-dicarboxy-2,2′-bipyridine)$_2$(NCS)$_2$] ("N3", Dyesol, B4 dye) in ethanol and then soaked in the dark for ∼24 h. They were subsequently removed from solution and rinsed with ethanol.

Platinized electrodes were prepared by cutting 2.5 × 2.5 cm squares from 15 Ω cm^{-2} glass (Hartford Glass) and sonicating in water and detergent for 15 min, followed by rinsing with water and 0.1 M HCl in ethanol and sonicating in acetone. Electrodes were then heated at 400 °C for 20 min to remove organic residues. 25 μL of 5 mM H_2PtCl_6 in ethanol was spread over the surface of each electrode, and they were placed into an oven at 380 °C for 20 min and then cooled in ambient. Electrical contacts were made to each electrode using silver epoxy (Chemtronics) to attach tinned copper wire after removing the TiO_2 blocking layer from the photoanodes.

Shuttle Synthesis. Synthesis of redox shuttles was carried out according to literature procedures.[18,19] Unsubstituted 1,10-phenanthroline, 5-chloro-1,10-phenanthroline, 5-methyl-1,10-phenanthroline, and 5-nitro-1,10-phenanthroline were used as received from Aldrich. 3 equiv of phenanthroline ligand was dissolved in a minimal amount of 99.8% methanol with stirring. 1 equiv of $Co(ClO_4)_2 \cdot 6H_2O$ (Aldrich) was added, precipitating a light yellow solid in each case. The mixture was stirred for 2 h at 65 °C, after which time diethyl ether was added to the mixture to precipitate the product. The product, a yellow powder, was separated via vacuum filtration.

After synthesis, oxidized forms of each complex were isolated. The divalent compounds were dissolved in minimal acetonitrile and oxidized with excess $NOBF_4$. The BF_4^- ion was displaced by ClO_4^- with excess $LiClO_4$, and the resulting oxidized perchlorate salt was precipitated with ether and vacuum filtered. Shuttle solutions were prepared with each complex in γ-butyrolactone

(18) Sapp, S. A.; Elliott, C. M.; Contado, C.; Caramori, S.; Bignozzi, C. A. *J. Am. Chem. Soc.* **2002**, *124*, 11215–11222.
(19) Nelson, J. J.; Amick, T. J.; Elliott, C. M. *J. Phys. Chem. C* **2008**, *112*, 18255–18263.
(20) Liberatore, M.; Burtone, L.; Brown, T. M.; Reale, A.; Di Carlo, A.; Decker, F.; Caramori, S.; Bignozzi, C. A. *Appl. Phys. Lett.* **2009**, *94*, 173113−1–3.
(21) Nusbaumer, H.; Moser, J.-E.; Zakeeruddin, S. M.; Nazeeruddin, M. K.; Gratzel, M. *J. Phys. Chem. B* **2001**, *105*, 10461–10464.
(22) At the same time, they have shortcomings—most notably, anomalously slow diffusion through nanoparticle-based photoelectrodes, resulting in mass-transport attenuation of photocurrents.[19] These shortcomings conceivably could be addressed either by employing higher extinction dyes and thinner photoelectrodes or by turning to higher porosity photoelectrode architectures. See, for example: (a) Hamann.; et al. *Adv. Mater.* **2008**, *20*, 1560–1564. (b) Hamann.; et al. *J. Phys. Chem. C* **2008**, *112*, 10303–10307.
(23) Hamann, T. W.; Gstrein, F.; Brunschwig, B. S.; Lewis, N. S. *Chem. Phys.* **2006**, *326*, 15–23.
(24) Klahr, B. M.; Hamann, T. W. *J. Phys. Chem. C* **2009**, *113*, 14040–14045.

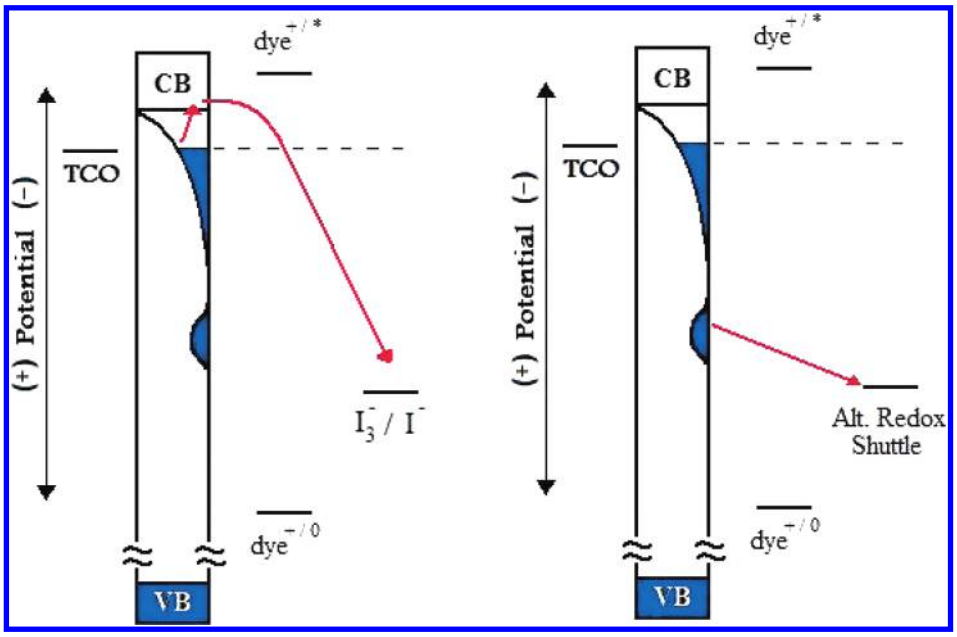

Figure 2. Schematic diagram of interception pathways entailing (a) thermal promotion to the conduction band before transfer to the shuttle and (b) direct transfer via sub-bandedge surface states.

(Aldrich). Solutions consisted of 0.135 M divalent cobalt complex, 0.015 M oxidized cobalt complex, and 0.15 M $LiClO_4$.

Cell Assembly and Photoelectrochemical Characterization. In order to eliminate variation in cell performance due to differences from electrode to electrode, the same platinized electrode was used for each measurement, and each TiO_2 electrode was reused in the following manner: a hole with area slightly larger than that of the TiO_2 films was punched in a piece of 25 μm Surlyn. The Surlyn was placed onto the platinized electrode as a spacer, and a glass pipet was used to dab a small amount of the electrolyte solution onto the hole. The TiO_2 electrode was then sandwiched onto it and held there by two metal clips on opposing sides of the electrode, taking care to ensure there were no bubbles in the film. After photoelectrochemical measurements were collected, the electrodes were unclipped, rinsed, and soaked with γ-butyrolactone before rinsing and soaking in ethanol for 4−5 min. They were then dried under an N_2 stream and loaded with the next electrolyte solution.

Cyclic voltammetry of mediator solutions was performed on a CH Instruments CHI 900 electrochemical analyzer using a Ag/AgCl pseudoelectrode as reference, platinum disk counter electrode, and platinum wire working electrode at a scan rate of 100 mV/s. Photoelectrochemical measurements were carried out with a CH Instruments CHI 1202 electrochemical analyzer interfaced with a Jovin Yvon Spex FluoroLog-3 fluorimeter equipped with a 450 W ozone-free xenon lamp. The fluorimeter slit width and sample holder were positioned so as to set light intensity to 100 mW/cm^2 after passing through an AM 1.5 solar filter.

Results

Initially constructed cells exhibited photocurrent densities of ~1.5 mA cm^{-2} or less and relatively low open-circuit voltages, in accord with previous work reporting very low photocurrents for phenanthroline-based cobalt shuttles.[18] No clear pattern of reactivity based on the identity of phenanthroline substituents was evident. OCVD measurements yielded highly curved (rather than linear) plots of ln(time) vs voltage. Taken together, these observations are strongly suggestive of interception pathways that are dominated by direct reaction of trapped, sub-bandedge electrons with the redox shuttle. These pathways may be contrasted with pathways in which trapped electrons are first thermally promoted to the conduction band and then transferred to the shuttle (see Figure 2). For the latter, the driving force for the elementary electron transfer step is the difference in potential between the conduction bandedge and the redox shuttle. If the elementary step is rate-determining, then the dynamics of electron interception will vary as the potential of the redox shuttle is varied. We have previously observed, with ferrocenium/ferrocene couples, that this type of behavior can be engendered by intentionally passivating trap states via atomic layer deposition (ALD) of an insulating metal oxide such as alumina,[25] an effect first observed by the Bisquert group.[26] This approach is explored below.

Photoanode Modification. Upon coating the photoanode with alumina via a single ALD cycle (pror to dye adsorption), significant improvements in photocurrent and open-circuit voltage were observed: photocurrent densities increased by more than a factor of 2, and V_{oc} values increased by ~50 mV, albeit with decreased fill factors. (A single ALD cycle conformally deposits 70−80% of a monolayer of alumina. In our experience two or three cycles are needed to coat all titanium sites.) The diminished fill factors with high current are tentatively attributed to the slow reduction of cobalt polypyridyl redox shuttles at platinized cathodes.[18] Such improvements with passivating/blocking layers have been observed before in cells employing cobalt shuttles with TiO_2 photoanodes and alumina blocking layers prepared by a dip-coating procedure.[20]

As shown in Figure 3, deposition of progressively thicker coatings resulted in progressively smaller photocurrents—behavior we tentatively attribute to tunneling barrier effects such that electron injection becomes less efficient with thicker coatings. (Each cycle deposits, on average, 1.1 Å of alumina). As also illustrated by the figure, the open-circuit photovoltage (V_{oc}) at first increases with alumina coating but then decreases. The peaking behavior of the V_{oc} is likely the combined result of the continuing passivation of the surface and the elimination of

(25) Hamann, T. W.; Farha, O. K.; Hupp, J. T. *J. Phys. Chem. C* **2008**, *112*, 19756–19764.

(26) Fabregat-Santiago, F.; Garcia-Cañadas, J.; Palomares, E.; Clifford, J. N.; Haque, S. A.; Durrant, J. A.; Garcia-Belmonte, G.; Bisquert, J. *J. Appl. Phys.* **2004**, *96*, 6903–6907.

Table 1. Differences in Formal Potential from the Unsubsituted Complex, Observed Open-Circuit Voltages, and Quasi-Fermi Level Relative to the Potential of the Unsubstituted Complex[a]

	$Co(Me\text{-}phen)_3^{3+/2+}$	$Co(phen)_3^{3+/2+}$	$Co(Cl\text{-}phen)_3^{3+/2+}$	$Co(NO_2\text{-}phen)_3^{3+/2+}$	I_3^-/I^-
V_{oc} (V)	0.647	0.679	0.737	0.787	0.741
$\Delta E°$ (V)	−0.045		0.096	0.176	−0.039
quasi-Fermi level relative to potential for $Co(phen)_3^{3+/2+}$ (V)	−0.692	−0.679	−0.641	−0.611	−0.780

[a] While V_{oc} does increase with more positive $E°$, the lower values for the shuttles with more positive potentials after correcting for differences in $E°$ are indicative of a lowering of the quasi-Fermi level due to faster recombination, characteristic of Marcus normal-region behavior.

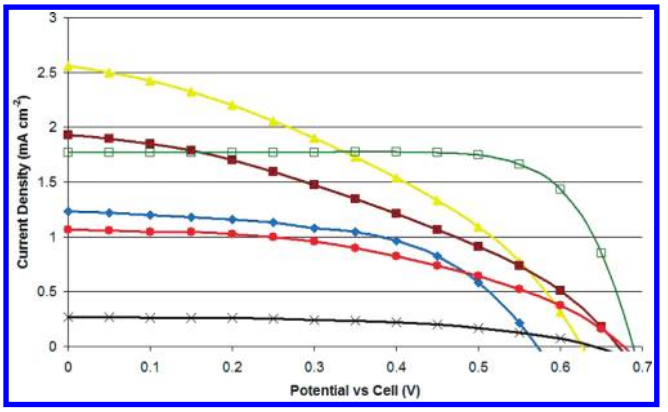

Figure 3. Photocurrent densities for cells employing the unsubstituted $Co(phen)_3^{3+/2+}$ mediator with 0 (blue diamonds), 1 (yellow triangles), 2 (maroon squares), 3 (red circles), and 5 (black crosses) cycles of alumina ALD. Photocurrent density plot of cells employing the I_3^-/I^- shuttle (green open squares) at one-fifth the light intensity (20 mW/cm^2) is included for comparison.

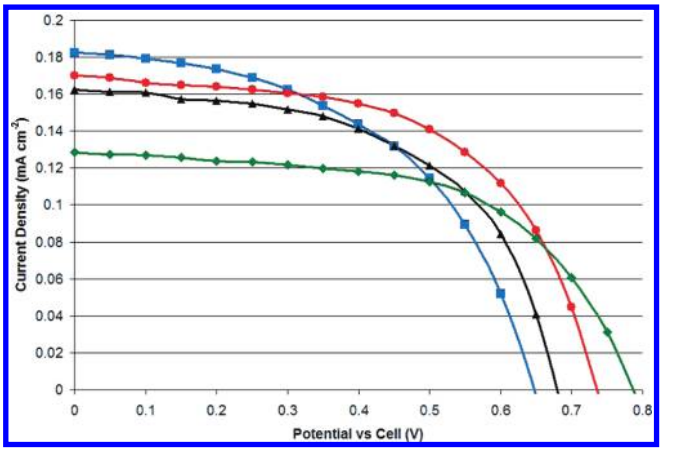

Figure 4. Photocurrent densities for cells coated with five cycles of alumina ALD and utilizing $Co(5\text{-methyl-phen})_3^{3+/2+}$ (blue squares), $Co(phen)_3^{3+/2+}$ (black triangles), $Co(5\text{-chloro-phen})_3^{3+/2+}$ (red circles), and $Co(5\text{-nitro-phen})_3^{3+/2+}$ (green diamonds) mediators.

recombination centers as additional ALD cycles are applied,[27] balanced against a growing tunneling barrier to electron interception with thicker layers of alumina. At some point (three or more ALD cycles) the surface is fairly free of these reactive surface states, and additional cycles of alumina provide little or no additional decrease in interception derived from continued passivation of these states, but instead merely serve as a thicker tunneling barrier to interception from the TiO_2. The decrease in injection rate through this barrier and the subsequently lower electron density in the TiO_2 then outstrips the increase in electron density from a tunneling barrier to interception, and the result is lower V_{oc} values. Because experiments with five cycles (5.5 Å) of alumina appear to be least affected by recombination contributions from surface states, most of the subsequent analysis will focus on photoanodes coated with 5.5 Å of alumina.

Shuttle Dependence of Photocurrent, V_{oc}, and Quasi-Fermi Level. Low photocurrents (~3 mA cm^{-2} or less) were observed for all cells. This pattern of low photocurrents with cobalt polypyridyl shuttles has been reported to be due to slow mass transport through the nanoparticle network[19] as well as poor charge collection efficiency due to relatively fast electron interception by the shuttle. It is worth noting, though, that there is not a pattern of sequentially lower photocurrents resulting from shuttles with more positive formal potentials, suggesting that insufficient driving force for dye regeneration is not a limiting factor.

The data show increases in V_{oc} as the formal potential of the redox shuttle becomes more positive, with the nitro-substituted shuttle showing open-circuit voltages over 0.8 V, with the highest achieving 0.844 V, albeit with low photocurrent.[28] This finding is notable, as previous efforts employing redox shuttles with more positive potentials such as $(SeCN)_2/SeCN^-$ and $(SCN)_2/SCN^-$ [29] and even $Co(phen)_3^{3+/2+}$ and $Co(5\text{-nitro-phen})_3^{3+/2+}$ shuttles were unsuccessful due in part to dramatic increases in dark current, resulting in very low V_{oc}, with the shuttles with more positive potentials performing worse.

In addition to variations in V_{oc}, we were interested in understanding how the quasi-Fermi level (at open circuit) varies with the identity and properties of the redox shuttle. A large portion of the variation in V_{oc} can be ascribed to changes at the dark electrode (i.e., changes in Co(III/II) formal potential). To compare quasi-Fermi levels, therefore, we referenced the energies to a single redox shuttle ($Co(phen)_3^{3+/2+}$) as shown in Table 1. We find that the open-circuit quasi-Fermi level drops (i.e., becomes less negative on an electrochemical energy scale) as the redox shuttle's potential increases (Figure 5). For the case where electron interception is dominated by recombination via the conduction band, we have previously shown that this type of behavior is indicative of Marcus normal-region behavior.[25] In other words, interception becomes faster as the overall driving force increases.[30] To our knowledge, the opposite case—Marcus inverted behavior—has yet to be unambiguously observed for electron interception reactions, although it is well-known for electron/dye recombination.[31−35]

(27) Bisquert, J.; Zaban, A.; Greenshtein, M.; Mora-Sero, I. *J. Am. Chem. Soc.* **2004**, *126*, 13550–13559.

(28) The best cells constructed in this study employed anodes coated with one ALD cycle of alumina, gold cathodes, and a concentrated solution of the $Co(5\text{-nitro-phen})_3^{3+/2+}$ mediator and showed J_{sc} of 1.96 mA cm^{-2}, V_{oc} of 0.79 V, FF of 0.489, and overall efficiencies of 0.76%.

(29) Oskam, G.; Bergeron, B. V.; Meyer, G. J.; Searson, P. C. *J. Phys. Chem. B* **2001**, *105*, 6867–6873.

(30) Marcus, R. A. *J. Chem. Phys.* **1956**, *24*, 966–978.

(31) Kuciauskas, D.; Freund, M. S.; Gray, H. B.; Winkler, J. R.; Lewis, N. S. *J. Phys. Chem. B* **2001**, *105*, 392–403.

(32) Gaal, D. A.; MacGarrah, J. E.; Liu, F.; Cook, J. E.; Hupp, J. T. *Photochem. Photobiol. Sci.* **2004**, *3*, 240–245.

(33) Gaal, D. A.; Hupp, J. T. *J. Am. Chem. Soc.* **2000**, *122*, 10956–10963.

(34) Dang, X.; Hupp, J. T. *J. Am. Chem. Soc.* **1999**, *121*, 8399–8400.

(35) Lu, H.; Preiskorn, J. N.; Hupp, J. T. *J. Am. Chem. Soc.* **1993**, *115*, 4927–4928.

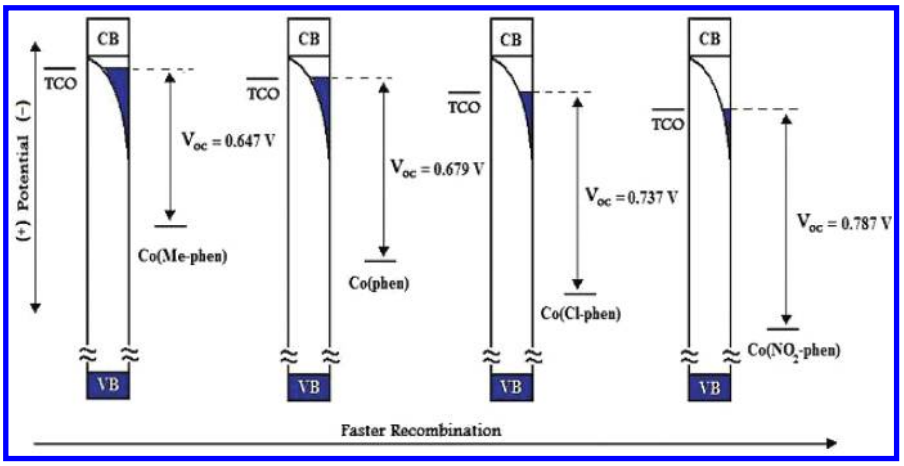

Figure 5. Trends in the shift in quasi-Fermi level as redox shuttles with more positive formal potentials are utilized in DSSCs. For a shuttle in the Marcus normal region, increasing the driving force for the interception reaction by making its formal potential more positive will increase the rate constant for interception and lower the quasi-Fermi level, decreasing gains in V_{oc}, as shown. Shuttles with more positive potentials exhibited greater V_{oc} but faster interception.

OCVD and Charge Carrier Lifetimes. Open-circuit voltage decay (OCVD) measurements were collected by holding the cell at open-circuit under illumination until the voltage reached steady state, then removing the light source, and monitoring the decay in cell voltage as electrons in the anode were intercepted by the redox shuttle. These data allow one to calculate the apparent charge lifetime in the cell, that is, the time (τ_n) that an injected electron survives before recombining with the redox shuttle at the interface. We employed the following equation:[36]

$$\tau_n = \frac{k_B T}{q}\left(\frac{dV_{oc}}{dt}\right)^{-1}$$

where k_B is Boltzmann's constant and q is the unit electronic charge.

The OCVD curves should be simple exponential decays if the dominant interception pathway in the cell is from the thermal population of the conduction band from the exponential distribution of traps,[37] as illustrated in the left-hand side of Figure 2. However, if another interception pathway significantly contributes, the OCVD curves will deviate from an exponential decay and charge lifetime plots will be nonlinear. In particular, if interception is dominated by monoenergetic deep trap states acting as recombination centers, OCVD curves would instead show linear behavior, corresponding to *potential-independent* charge lifetimes.[38] Shunting by direct electron transfer from an exposed FTO substrate to cobalt shuttles has been reported[39] as well as its similar effect on photovoltage decay and charge lifetime plots,[40] although in our case this possibility has been ruled out by the thick TiO_2 blocking layer used.

Shown in Figure 6a are OCVD curves for Co(phen)$^{3+/2+}$-containing cells featuring a sequence of photoelectrodes coated with alumina layers of various thicknesses. Shown in Figure 6b are log−linear plots of electron survival time versus cell voltage. Cells containing unmodified photoanodes exhibited fast interception and short charge lifetimes, with cell voltages decaying to nearly zero within a few seconds. OCVD curves for cells with one cycle of alumina showed very different behavior—decays that are clearly nonexponential. In the corresponding charge lifetime plots (Figure 6b), cells featuring 1.1 Å (only) of alumina display nearly potential-independent τ_n values over the range of 0.4−0.1 V. As indicated above, this behavior points to surface-state-mediated electron interception.

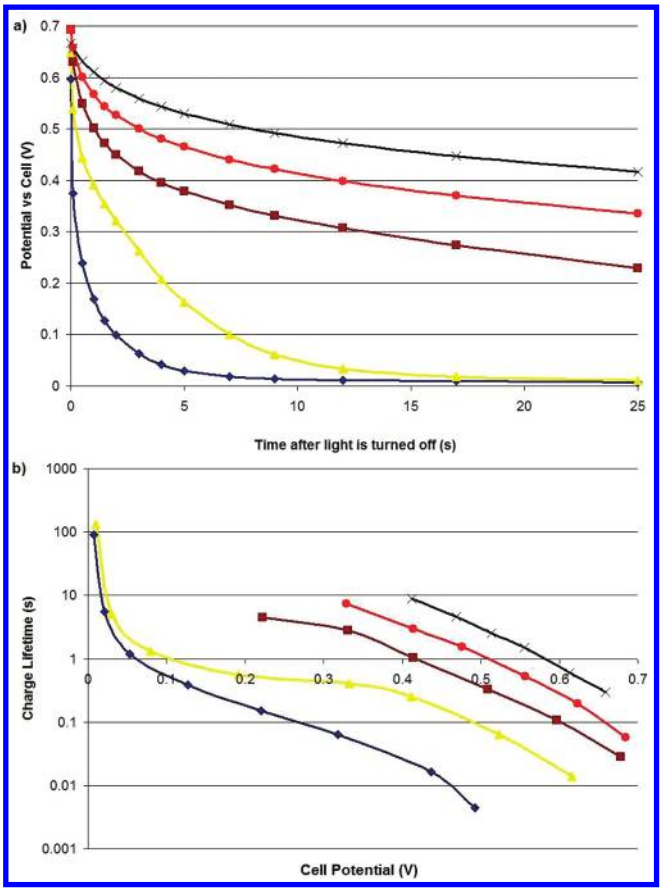

Figure 6. (a) OCVD curves and (b) charge lifetime plots for cells employing the unsubstituted Co(phen)$_3^{3+/2+}$ mediator with 0 (blue diamonds), 1 (yellow triangles), 2 (maroon squares), 3 (red circles), and 5 (black crosses) cycles of alumina ALD.

Better behaved OCVD curves, i.e., more nearly exponentially decaying curves, are seen with thicker alumina coatings (these

(36) Zaban, A.; Greenshtein, M.; Bisquert, J. *ChemPhysChem* **2003**, *4*, 859–864.
(37) Bisquert, J.; Vikhrenko, V. S. *J. Phys. Chem. B* **2004**, *108*, 2313–2322.
(38) Bisquert, J.; Zaban, A.; Salvador, P. *J. Phys. Chem. B* **2002**, *106*, 8774–8782.
(39) Cameron, P. J.; Peter, L. M.; Zakeeruddin, S. M.; Gratzel, M. *Coord. Chem. Rev*. **2004**, *248*, 1447–1453.
(40) Bailes, M.; Cameron, P. J.; Lobato, K.; Peter, L. M. *J. Phys. Chem. B* **2005**, *109*, 15429–15435.

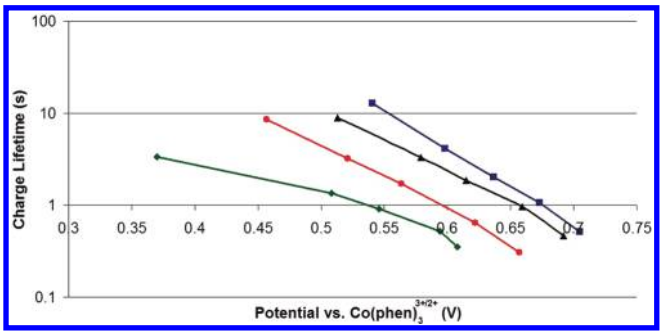

Figure 7. Charge lifetimes corrected for differences in redox potential for cells coated with five cycles of alumina ALD and utilizing Co(5-methyl-phen)$_3^{3+/2+}$ (blue squares), Co(phen)$_3^{3+/2+}$ (black triangles), Co(5-chloro-phen)$_3^{3+/2+}$ (red circles), and Co(5-nitro-phen)$_3^{3+/2+}$ (green diamonds) mediators.

data also exhibit the expected linear plots when the photovoltage decays vs ln(t) are plotted).[41] The corresponding charge lifetime plots (Figure 6b) are reasonably straight over an extended range of potentials, consistent with electron interception via the conduction band rather than directly via trap states.[42]

Figure 7 compares potential-dependent electron survival times as a function of the identity of the redox shuttle. In order to account for variations in potential at the counter electrode (due to variations in the identity of the redox shuttle), the data are presented versus the potential for Co(phen)$_3^{3+/2+}$, rather than as cell potentials. The plots show that at a given potential the survival times decrease in the order Co(5-methyl-phen)$_3^{3+/2+}$ > Co(phen)$_3^{3+/2+}$ > Co(5-chloro-phen)$_3^{3+/2+}$ > Co(5-nitro-phen)$_3^{3+/2+}$. In other words, electron interception is fastest when the driving force is highest; i.e., Marcus normal-region behavior is observed. This conclusion is not altogether unexpected, as Hamann et al. reported the Marcus normal behavior of Co(bpy)$_3^{3+/2+}$, observing the change in the rate constant for this electron transfer as the flat-band potential of a ZnO electrode was varied with solution pH.[23]

Finally, it may be useful to compare the OCVD behavior of dye cells featuring slow (triiodide/iodide), intermediate (Co(phen)$_3^{3+/2+}$), and fast (ferrocenium/ferrocene) electron-exchanging shuttles. This is done in Figure 8 where data are presented for photoelectrodes both with and without 5.5 Å alumina barrier layers. From the figure, it is evident that (a) electron survival times with the three shuttles are ordered as expected, (b) survival times with ferrocenium/ferrocene, at alumina-coated electrodes, are nearly as great as those seen with triiodide/iodide at native electrodes,[25] (c) survival times at unmodified electrodes are ca. 50−100-fold shorter in the presence of Co(phen)$_3^{3+/2+}$ than in the presence of triiodide/iodide, (d) survival times at alumina-coated

(41) Walker, A. B.; Peter, L. M.; Lobato, K.; Cameron, P. J. *J. Phys. Chem. B* **2006**, *110*, 25504–25507.

(42) While this paper was under review a related paper (Ondersma, J. W.; Hamann, T. W. *J. Phys. Chem. C* (DOI: 10.1021/jp908442p) was published. Based, in part, on impedance measurements, they conclude that the dominant effect of alumina layers (or even a single layer) is that of a tunneling barrier, rather than passivation of surface states. We agree that the dominant effect of thicker layers of alumina (i.e., three or more cycles) is that of a tunneling barrier; our data seem to indicate, for thinner coatings, an important role for surface-state passivation.

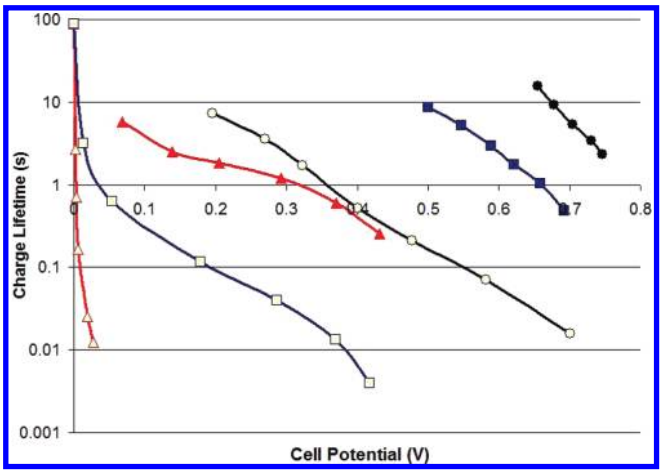

Figure 8. Comparison of charge lifetimes with various shuttles with no barrier layer (open symbols) and five ALD cycles of alumina (closed symbols). Charge lifetimes with the ferrocenium/ferrocene (red triangles), Co(phen)$_3^{3+/2+}$ (blue squares), and I_3^-/I^- (black circles) mediators are shown.

electrodes in the presence of Co(phen)$_3^{3+/2+}$ are ca. 50-fold longer than at native electrodes in the presence of triiodide/iodide, and (e) the full range of electron survival times at a given cell potential can be made to span several orders of magnitude, depending on the identity of the shuttle and the presence (or not) of an alumina barrier layer. Unfortunately, 5.5 Å barrier layers significantly inhibit electron injection, resulting in low photocurrents. Going forward, it would appear desirable to develop dyes possessing longer lifetimes and/or intrinsically faster electron-injection kinetics so that the otherwise beneficial effects of barrier layers could be fully exploited.

Conclusions

ALD-based alumina modification photoanodes enables a systematic approach to the study of alternatives to the I_3^-/I^- couple in dye-sensitized solar cells. One-electron couples, previously exhibiting typically poor performance due to facile interception of injected electrons through reactive surface states, may now be utilized in cells without this limitation, allowing for a systematic investigation. Application of this strategy to Co(phen)$_3^{3+/2+}$ and its derivatives shows that, at modified electrodes, electron recombination with the shuttle occurs via the conduction band, rather than directly via surface states. The interception reactions take place in the Marcus normal region as evidenced by increased rates of interception as the reaction driving force is increased. With alumina-modified electrodes, photovoltages greater than 0.8 V have been obtained, albeit at the cost of diminished electron injection efficiencies and concomitant loss of photocurrent.

Acknowledgment. We thank Dr. Alex Martinson for helpful discussions. We gratefully acknowledge the U.S. Department of Energy's Office of Science (Grant DE-FG87ER13808) and Argonne National Laboratory for financial support of our research.